International Forum on Aeroelasticity and Structural Dynamics
IFASD 2024
17-21 June 2024, The Hague, The Netherlands

AEROELASTIC ANALYSIS OF A SMART SMA-COMPOSITE WING

Gefferson C. Silva[1], Flavio J. Silvestre[1], Mauricio V. Donadon[2]

[1]Technical University of Berlin
Marchstraße 12, 10587 Berlin, Germany
g.silva@tu-berlin.de
flavio.silvestre@tu-berlin.de

[2]Aeronautical Institute of Technology
Marechal E. Gomes Square 50, 12228900 Sao Jose dos Campos, Brazil
donadon@ita.br

Keywords: SMA, nonlinear aeroelasticity, structural dynamics, smart structures

Abstract: The present work reports on the development of a numerical aerothermoelastic tool that accounts for nonlinearities of multi-physical sources to investigate the behavior of flexible wings made of a hybrid smart material. Here, hybrid materials consist of laminated composites reinforced with embedded shape memory alloy wires. The proposed model gathers geometrical, material, and aerodynamic nonlinearities to the thermal heating dynamics of SMA wires via the Joule effect. To this end, a geometrically nonlinear FE beam model is coupled with material nonlinearities via a micromechanical model that computes the homogenized properties of hybrid laminates. Nonlinear aerodynamic effects are introduced through an unsteady strip theory method in the time domain, along with the assumption of follower aerodynamic forces and a quasi-steady stall model. A set of aerothermoelastic cases was simulated by assuming various layups and SMA temperatures to tailor and analyze the aeroelastic response of hybrid wings. The outcomes have shown a considerable reduction in post-flutter oscillations as the SMA temperature increases, indicating evidence of the capability of hybrid materials for aeroelastic applications.

1 INTRODUCTION

Despite the recent COVID-19 Pandemic crisis, the aviation field has been still experiencing an expansion process, establishing this sector as one of the major vectors of every nation's economy. However, the triumph of this business is connected with a wide range of environmental damages, such as the augmented emissions of greenhouse gases. Therefore, the concept of 'green aircraft' has been attracting interest in the aeronautical scenario in the last decades, playing an important role in establishing a new aircraft generation that also grants ecological advantages. Diverse efforts have been dedicated to enhancing the aircraft's overall performance by combining novel structural and aerodynamic concepts with the use of modern materials. High aspect-ratio wings, along with the usage of composite materials, are worthwhile forms to attain these requirements.

Lately, advances in material technologies have been also pushing forward to the use of smart composites in many phases of aircraft structural design. This is done in order to optimize the vehicle's structural response, reducing its weight and contributing to minimize fuel consumption and hence emissions. For this matter, a material that presents standout attributes is the shape

memory alloy, or just SMA. This material has drawn much attention in different areas, with applications ranging from cardiovascular procedures [1] to aerospace missions [2]. SMAs also offer an attractive combination of energy density, great resistance, and control capabilities, as discussed in [3].The most reported use of SMAs within aeronautics concerns wing morphing cases, wherein these alloys are applied to alter the geometrical characteristics of wing sections, as per done in [4, 5].

The key reason that substantiates SMAs to succeed in different areas of application is related to their mechanical-thermal interactions that confer unique properties to the host system, such as the shape memory effect, the pseudo-elastic effect, and the stiffening-induced effect [6]. The latter is produced by the fact that the austenite crystallographic phase (or high temperature phase) provides a stiffness higher than the one produced by a state of pure martensite (or low temperature phase). This feature permits 'smart applications' with adaptive characteristics [7], including the present work. This material may still offer a high reliability and a striking reduction of the overall system mass, as emphasized in [8].

Numerous works have employed SMAs to examine the aeroelastic behavior of the so-called hybrid SMA-composite structures, or just hybrid composites. In these cases, the assumption of a structure made of a composite material with embedded SMA wires is held, and the SMA stiffening-induced effects are supposed to change the aeroelastic behavior of the host structure. The great majority of these studies have embraced numerical flutter analyses of hybrid panels undergoing supersonic loads. In addition, few works have investigated the structural and aeroelastic responses of composite structures mutually reinforced by both fibers and SMA wires. Commonly, the literature treats hybrid materials as compounded only by a polymeric matrix reinforced by SMA materials, whereas fiber-like reinforcements are disregarded.

Despite recent growth in this area, the development of SMA-composite materials present an absence of deeper investigations and demand for clarification, as stated by Jani *et al.* [9] in a review of applications and opportunities within SMA-based researches. Moreover, another concern here is the lack of numerical tools capable of predicting the behavior of hybrid structures accurately. Therefore, aiming at reducing this gap of evidence, this work brings forward an aeroelastic model of hybrid beams that accounts for multi-physical nonlinearities, the so-called nonlinear aerothermoelastic model herein. Also, the present study enlarges the modeling of such materials by coupling a thermal dynamics of SMAs and by assuming wings made of a polymeric resin with both embedded fibers and SMA wires, as shown in Fig. 1.

Geometrical nonlinearities are accounted for by the assumption of a plane, Timoshenko's beam under large deformations. Material nonlinearities are enclosed via semi-empirical micromechanical and thermoelastic models of hybrid structures. Nonlinear aerodynamic effects are taken into account via a quasi-steady stall model combined with the assumption of follower aerodynamic forces, both included into an unsteady strip theory model in the time-domain. The final set of nonlinear aerothermoelastic equations is solved by using a combination of Newmark's and Newton-Raphson methods. As early announcements, the findings indicated evidence of such materials to reduce post-flutter oscillation amplitudes when applied to aerostructures. These results substantiate embedded SMAs as a worthwhile method for aeroelastic control of slender wings.

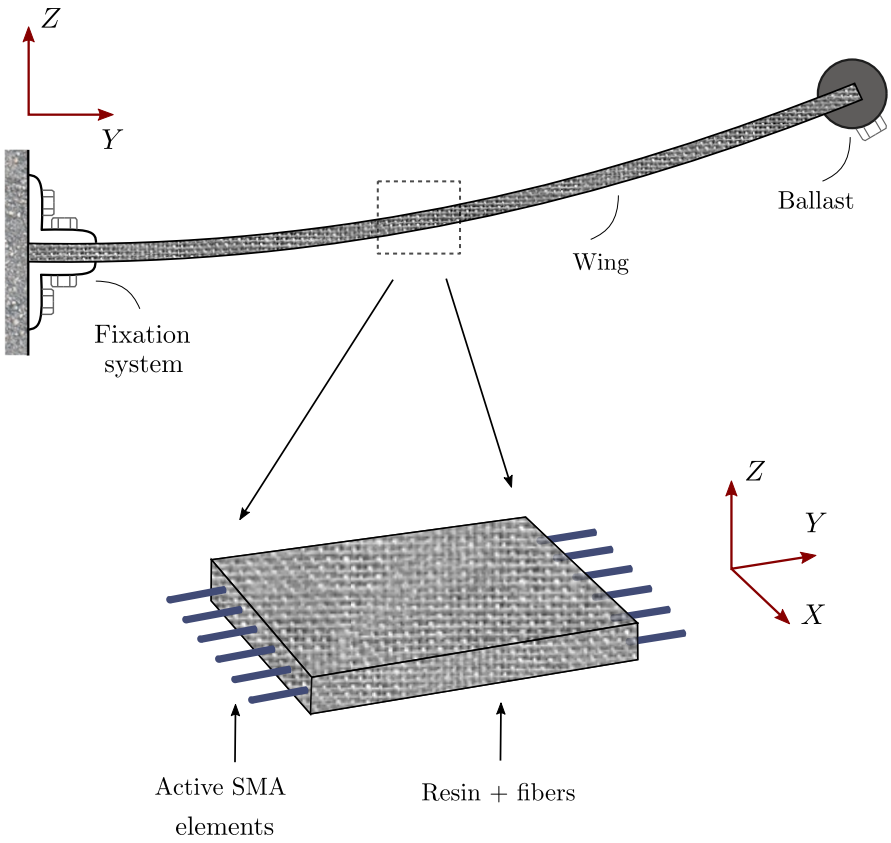

Figure 1: High aspect-ratio hybrid SMA-composite wing with a ballast at the tip.

2 NONLINEAR MODEL

The applicability horizon of linear models applied for engineering solutions is defined by the target phenomenon *per se*. This assertion is instantiated by the suit that the accuracy of findings, either based on qualitative or quantitative metrics, is directly connected with the level of refinement used in the mathematical formulation of the problem. As a result, elaborate phenomena may claim for nonlinear descriptions. A great example is the modern fluid-structure analysis of flexible wings, in which multiple complex disciplines and effects are involved.

The work at hand conducts an intrinsically nonlinear problem, the aerothermoelastic problem of flexible composite wings with embedded shape memory alloys. Therefore, the mathematical formulation employed to derive this nonlinear model is presented, starting with the structural formulation, passing through the aerodynamic and thermal models, and moving up to the numerical solution method.

2.1 Structural Model

The kinematics of a Timoshenko beam is calculated under the assumption of large bending deflections, along with a homogeneous linear torsion model. Consider then a generic material particle located at $P(X, Y, Z)$ in the initial configuration $\mathcal{C}_0$ that moves to $p(x, y, z)$ in the current configuration $\mathcal{C}$ due to deformation, as illustrated in Fig. 2.

After a consistent-linearization technique for small-strains, as performed in [10], the nonlinear

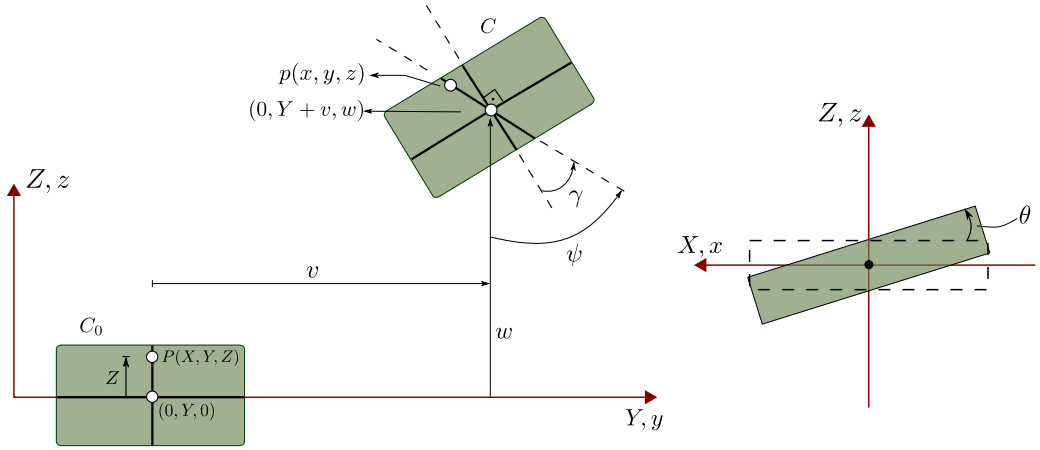

Figure 2: Kinematics of a Timoshenko's beam under large bending deflections.

set of relations between strains and deformations is collected in the strain vector $\boldsymbol{\epsilon}$, as:

$$\boldsymbol{\epsilon} = \left\{ \begin{array}{c} e_{yy} \\ \kappa_{yy} \\ \kappa_{xy} \\ \gamma_{yz} \end{array} \right\} = \left\{ \begin{array}{c} (1+v')\cos\psi + w'\sin\psi - 1 \\ \psi' \\ \theta' \\ -(v'+1)\sin\psi + w'\cos\psi \end{array} \right\}, \tag{1}$$

where $v(Y)$ and $w(Y)$ are the components of the neutral axis displacements referred to XYZ, $\psi(Y)$ is the cross-section rotation angle, and $\theta(Y)$ is the twisting angle.

The linearization is based upon the polar decomposition analysis of the deformation gradient. As an outcome, all quantities are limited to first-order polynomial terms, except for the trigonometrical dependencies of the cross-section rotation angle ψ. The resulting non-zero strain components are the membrane strain e_{yy}, the bending curvature κ_{yy}, the in-plane shear strain κ_{xy} (due to torsion), and the transverse shear strain γ_{yz}.

2.2 Thermoelasticity of SMA Wires

The elastic response of SMA materials - exhibiting the stiffening-induced effect - is introduced here on the basis of the studies reported by Aquino *et al.* [11] and by Donadon and Faria [12]. This effect arises from the thermal cycling of SMAs to temperatures above and below their phase transformation temperatures, under isostrain conditions. In detail, the internal stress distribution is modified for temperatures between those involved in the phase transformations. Meanwhile, the strains are kept constant or present an insignificant variance, which results in a substantial modification of the material elastic moduli.

The referred model establishes a correspondence between the operating SMA temperature T, the austenitic start temperature (A_S), the austenitic finish temperature (A_F), and the material constant β. The latter is associated with the rate at which such transformation occurs. These quantities are thus related as

$$\begin{aligned} E_{sma}(T) &= E^M_{sma} + \Big(1 - \xi_M(T)\Big) E^A_{sma} \\ &= E^M_{sma} + \xi_A(T) E^A_{sma}\,, \\ G_{sma}(T) &= \frac{E_{sma}(T)}{2\,(1-\upsilon_{sma})}\,, \end{aligned} \tag{2}$$

where E_{sma}^{M} and E_{sma}^{A} are the respective SMA Young's moduli regarding the martensite and austenite phases, υ_{sma} is the SMA Poisson's ratio, and E_{sma} and G_{sma} are the temperature-dependent SMA Young's modulus and the in-plane shear modulus, respectively.

With the thermo-mechanical relation of SMA wires, attention is now turned to predicting the mechanical response of hybrid laminates. Several techniques are available to forecast the elastic behavior of laminates reinforced by aligned long-fibers. The most successful of those is the semi-empirical method proposed by Halpin and Tsai [13], which is applied in this work to compute the elastic properties of a hybrid lamina. However, the classical Halpin-Tsai equations are not promptly applicable to composites with multiple reinforcements. Therefore, as two different reinforcements are assumed here, the Halpin-Tsai equations must be employed twice.

The resin, fibers, and SMA phases are assumed to have volume fractions given by V_m, V_f, and V_{sma}, respectively. Then, the overall elastic properties of a lamina compounded of SMA/(fiber/matrix) can be computed as

$$\begin{aligned} E_2(T) &= {E_2}' \left(\frac{1 + \xi_2 \eta_2(T) V_{sma}}{1 - \eta_2(T) V_{sma}} \right) , \\ G_{12}(T) &= {G_{12}}' \left(\frac{1 + \xi_{12} \eta_{12}(T) V_{sma}}{1 - \eta_{12}(T) V_{sma}} \right) , \\ G_{23}(T) &= {G_{23}}' \left(\frac{1 + \xi_{23} \eta_{23}(T) V_{sma}}{1 - \eta_{23}(T) V_{sma}} \right) , \\ G_{13}(T) &= G_{12}(T) , \end{aligned} \tag{3}$$

where

$$\begin{aligned} \eta_2(T) &= \frac{E_{sma}(T)/{E_2}' - 1}{E_{sma}(T)/{E_2}' + \xi_2} , \\ \eta_{12}(T) &= \frac{G_{sma}(T)/{G_{12}}' - 1}{G_{sma}(T)/{G_{12}}' + \xi_{12}} , \\ \eta_{23}(T) &= \frac{G_{sma}(T)/{G_{23}}' - 1}{G_{sma}(T)/{G_{23}}' + \xi_{23}} , \end{aligned} \tag{4}$$

and

$$\begin{aligned} \xi_2 &= 2 + 40 {V_{sma}}^{10} \approx 2 , \\ \xi_{12} &= 1 + 40 {V_{sma}}^{10} \approx 1 , \\ \xi_{23} &= \frac{{E_2}'/2{G_{12}}' \left(1 - {\upsilon_{12}}' - 2{\upsilon_{12}}'^2\right)}{{E_2}'/2{G_{12}}' \left(1 - {\upsilon_{12}}' - 2{\upsilon_{12}}'^2\right) + 2} . \end{aligned} \tag{5}$$

Here, the superscript $(\ )'$ refers to the elastic properties of the fiber/matrix composition. The quantities E_f and E_m are, respectively, the fiber and matrix Young's moduli, whereas G_f and G_m are the analogous in-plane shear moduli. Moreover, υ_m and υ_f are the respective matrix and fiber Poisson ratios, and $E_{sma}(T)$ and $G_{sma}(T)$ are the Young's and shear moduli of the SMAs. To complement, the longitudinal Young's modulus $E_1(T)$, Poisson's ratio υ_{12}, and density ρ can be calculated similarly to the Rule of Mixtures.

Finally, by admitting a laminate beam consisting of orthotropic hybrid laminae and stacked sequentially, the material stiffnesses $EA(T)$, $EI(T)$, $GJ(T)$, $kGA(T)$ and the coupling terms $K_{bm}(T)$, $K_{mt}(T)$ and $K_{tb}(T)$ become temperature dependent. These parameters represent the membrane stiffness, the bending stiffness, the twisting stiffness, and the transverse shear stiffness of a hybrid beam, respectively. In addition, the coupling terms are the bending-membrane coupling stiffness, the membrane-torsion stiffness, and the torsion-bending stiffness. Coupling terms are resulting from anisotropic characteristics of laminated composite beams.

Figure 3 depicts the coupling terms response to a variation of the SMA operating temperature T. For this purpose, it was assumed a five-layer hybrid beam with unsymmetrical layup $[45/0/90/-25/-45]$, layer thickness $t_k = 0.19$ mm, constituents volume fractions $V_f = V_{sma} = 25\%$ and $V_m = 50\%$, and constituents mechanical properties shown in Table 1.

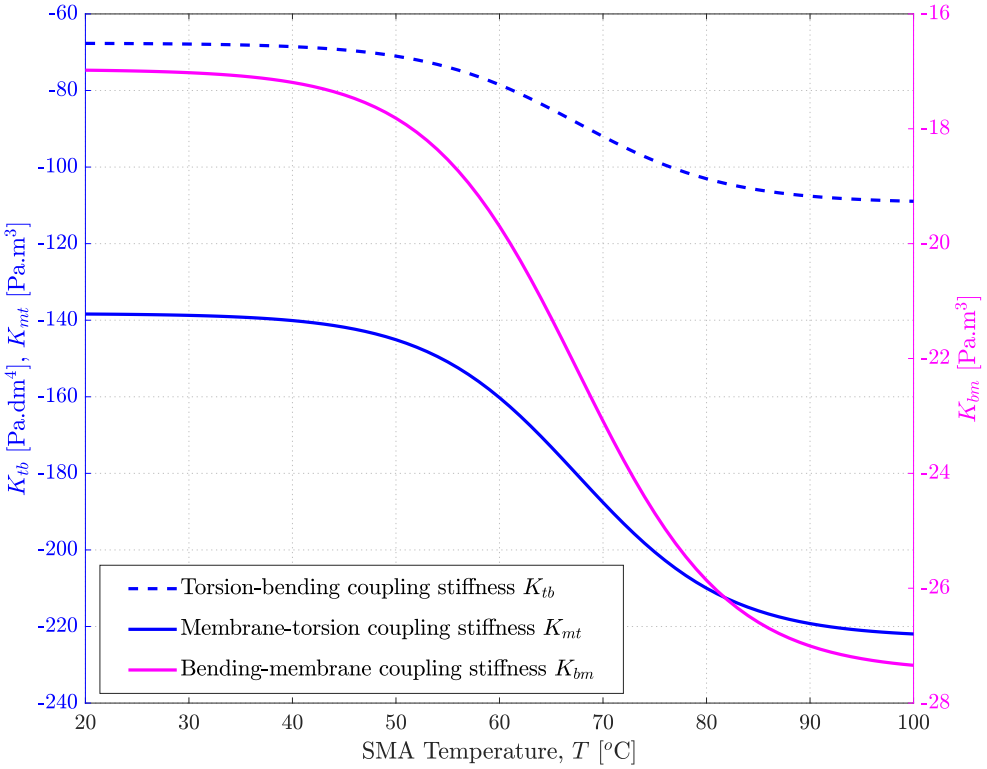

Figure 3: Variation of the coupling-stiffness parameters with the temperature.

Table 1: Mechanical properties of a hybrid lamina.

Carbon fiber		**Epoxy resin**		**Ni-Ti wire**		**Unit**
E_f	129	E_m	2	E^M_{sma} - E^A_{sma}	30 - 95	GPa
υ_f	0.3	υ_m	0.3	υ_{sma}	0.3	-
ρ_f	1750	ρ_m	1200	ρ_{sma}	6450	kg/m^3
				A_S - A_F	45 - 90	°C

2.3 Aerodynamic Model

This section describes the premises for determining the aerodynamic loads undergone by hybrid wings. For that, Wagner's theory [14] is employed to represent the unsteady loads acting on a discretized wing experiencing arbitrary motion. A time-domain aerodynamic description is obtained by applying the Jones' approximation for Wagner's indicial function [15]. Furthermore,

the Yates' Modified Strip Theory [16] is used to accounting for aerodynamic effects of either stall or finite span. At last, effects of large deformations are computed through the hypothesis of follower aerodynamic forces.

Assuming a slender wing flying at airspeed V, the unsteady aerodynamic forces acting on a generic strip can be written as [17]

$$l_j^{aer}(t) = \left\{ \pi \rho_a b_j^2 \left(-\ddot{w}_j + V\dot{\theta}_j - b_j a_j \ddot{\theta}_j \right) + C_{l\alpha j} \rho_a V b_j \left[Q_{3/4j}(t) + \lambda_{1j}(t) + \lambda_{2j}(t) \right] \right\} \Delta y_j \,, \tag{6}$$

$$\begin{aligned} m_j^{ea}(t) = \Bigg\{ & \pi \rho_a b_j^2 \left[-V\dot{w}_j - b_j a_j \ddot{w}_j + V^2 \theta_j - b_j^2 \left(\frac{1}{8} + a_j^2 \right) \ddot{\theta}_j \right] \\ & - \pi \rho_a V b_j^2 \left[Q_{3/4j}(t) \right] + b_j \left(a_j - a_{cj} \right) l_j^{aer(c)}(t) \Bigg\} \Delta y_j \,, \end{aligned} \tag{7}$$

where Δy_j is the local width, b_j is the local chord, a_{cj} is the local aerodynamic center position (in semi-chords), and a_j is the local elastic axis position (in semi-chords). Additionally, λ_{1j} and λ_{2j} represent the aerodynamic lags, which can be given by solving the two following first-order differential equations:

$$\begin{aligned} \dot{\lambda}_{1j}(t) &= -0.0455 \frac{V}{b_j} \lambda_{1j}(t) - 0.165 \dot{Q}_{\frac{3}{4}j}(t) \,, \\ \dot{\lambda}_{2j}(t) &= -0.3000 \frac{V}{b_j} \lambda_{2j}(t) - 0.335 \dot{Q}_{\frac{3}{4}j}(t) \,, \end{aligned} \tag{8}$$

in which $Q_{3/4j}$ is the downwash at the local three-quarter chord position.

Within the assumption of follower forces, both bending and twisting rotations are admitted to modify the local lift on each strip. This effect is quantified by a transformation matrix as

$$\mathbf{f^{aer}}_j = \mathbf{r^{gl}}_j \begin{Bmatrix} 0 \\ l_j^{aer} \\ 0 \\ m_j^{ea} \end{Bmatrix} . \tag{9}$$

As a direct consequence of decomposing the lift vector, an additional force component of aerodynamic nature emerges in the longitudinal direction of the wing. Furthermore, the pitching moment does not appear to change, since the strip sections remain perpendicular to the correspondent lift vectors after deformation. To complement, the aerodynamic center position of each strip is assumed to not vary within the current supposition.

In order to complete the present nonlinear aeroelastic modeling, a quasi-steady $C_{l\alpha}$ distribution is applied here, as shown in Fig. 4. The referred curve was experimentally obtained by Pelletier and Mueller [18], in a study of thin flat plates with thickness-to-chord equal to 1.93%, which is similar to the thickness-to-chord relation of about 2.02% presented by the wings tested in this study.

At this point, the aerodynamic loads acting on each strip of a hybrid beam-like wing, accounting

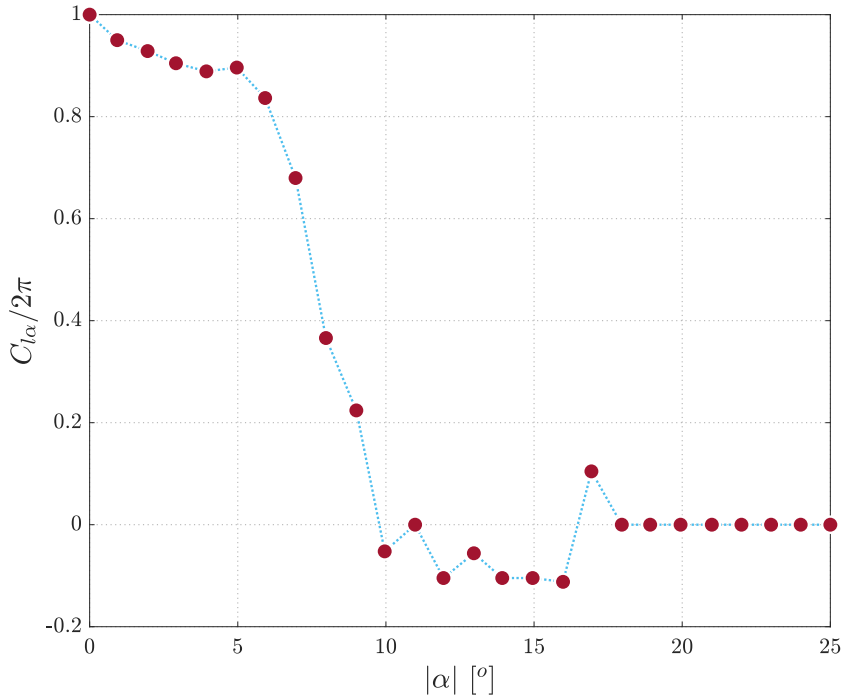

Figure 4: Variation of the lift-curve slope.

for the stall and follower forces models, can be expressed as

$$\mathbf{f^{aer}}_j = \mathbf{r^{gl}}_j \left\{ \mathbf{a_{1j}} \begin{Bmatrix} \ddot{v}_j \\ \ddot{w}_j \\ \ddot{\psi}_j \\ \ddot{\theta}_j \end{Bmatrix} + \mathbf{a_{2j}} \begin{Bmatrix} \dot{v}_j \\ \dot{w}_j \\ \dot{\psi}_j \\ \dot{\theta}_j \end{Bmatrix} + \mathbf{a_{3j}} \begin{Bmatrix} v_j \\ w_j \\ \psi_j \\ \theta_j \end{Bmatrix} + \mathbf{a_{4j}} \begin{Bmatrix} \lambda_{1j} \\ \lambda_{2j} \end{Bmatrix} \right\} \Delta y_j \,, \tag{10}$$

with the following associated lag states dynamics

$$\begin{Bmatrix} \dot{\lambda}_{1j} \\ \dot{\lambda}_{2j} \end{Bmatrix} = \mathbf{b_{1j}} \begin{Bmatrix} \ddot{v}_j \\ \ddot{w}_j \\ \ddot{\psi}_j \\ \ddot{\theta}_j \end{Bmatrix} + \mathbf{b_{2j}} \begin{Bmatrix} \dot{v}_j \\ \dot{w}_j \\ \dot{\psi}_j \\ \dot{\theta}_j \end{Bmatrix} + \mathbf{b_{3j}} \begin{Bmatrix} v_j \\ w_j \\ \psi_j \\ \theta_j \end{Bmatrix} + \mathbf{b_{4j}} \begin{Bmatrix} \lambda_{1j} \\ \lambda_{2j} \end{Bmatrix} , \tag{11}$$

wherein $\mathbf{a_{(1\ldots4)j}}$ and $\mathbf{b_{(1\ldots4)j}}$ are the local aerodynamic matrices.

2.4 SMA Wires under Joule's Effect

A thermal dynamic model that captures the slow heating process of SMA wires under Joule's effects is coupled to the nonlinear aeroelastic model. For that, thermal interactions between SMAs and the environment are also assumed to affect the SMA temperature. Therefore, by considering the SMA internal temperature $T(t)$ uniform throughout the wire, the room temperature T_{env} constant and uniform, and an electric current $i(t)$ passing through the SMA wire, the following differential expression can be found:

$$\tau_T \dot{T}(t) + T(t) = R_r i^2(t) + T_{env} \,, \tag{12}$$

where τ_T is the heating time constant, and R_r is the thermal-electric transduction constant.

Figure 5 - (a) displays the outcomes of the thermal dynamic equation above by considering $\tau_T = 30$ s, $R_r = 10$ °C/A^2, $T_{env} = 24$ °C, initial condition $T(0) = T_{env}$. Moreover, it is worth-mentioning that these values for the thermal parameters are applied in all aerothermoelastic cases hereafter.

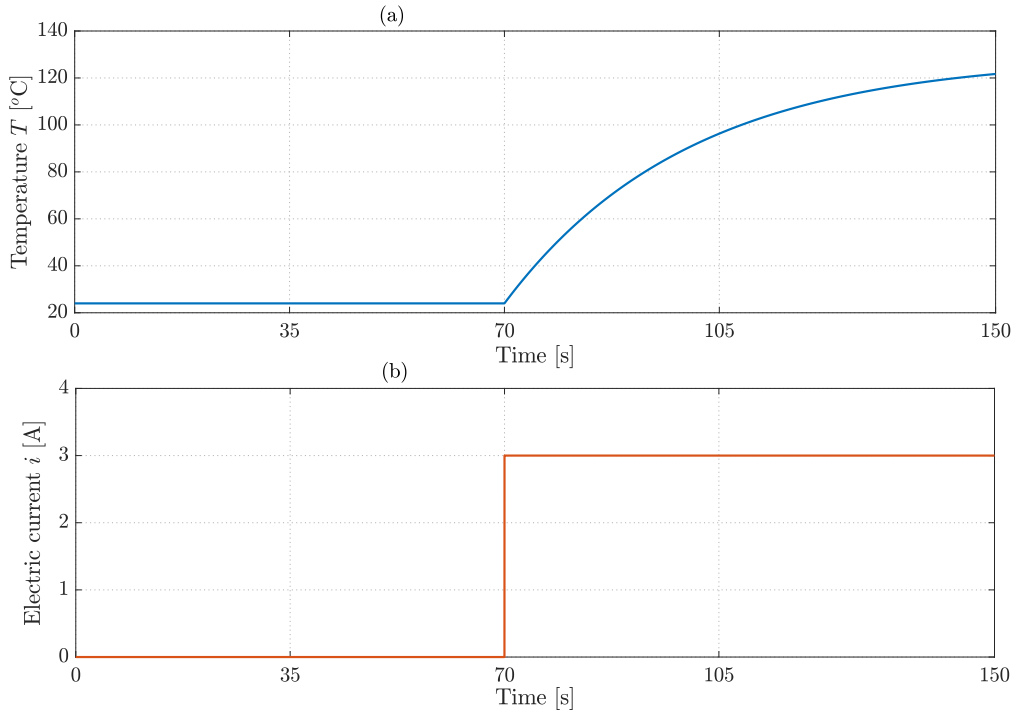

Figure 5: (a) - Thermal response of the SMA wires; (b) - Input in the electric current.

2.5 Aerothermoelastic Model

The so-called nonlinear aerothermoelastic problem of hybrid wings is defined in this section. To this end, an FE model that uses a 2D Timoshenko beam element with two-nodes is employed. This element presents 8 degrees of freedom, 4 per node, given by the axial displacement v, the out-of-plane bending deflection w, the internal cross-section rotation angle ψ, and the torsional angle θ.

Finally, by gathering structural, aerodynamic, and material nonlinearities with the thermal dynamics of SMA wires, in a matrix form, an extended set of nonlinear equations of motion can be formulated. Therefore, assuming a rectangular clamped-free hybrid beam-like wing with a ballast attached to its tip and undergoing a subsonic flow with speed V, results

$$\begin{bmatrix} \left[\mathbf{M} - \mathbf{R}^{\mathbf{gl}}(\tilde{\mathbf{d}})\mathbf{A_1}\right] & \mathbf{0} & 0 \\ -\mathbf{B_1}(\tilde{\mathbf{d}}) & \mathbf{0} & 0 \\ \mathbf{0} & \mathbf{0} & 0 \end{bmatrix} \begin{Bmatrix} \ddot{\tilde{\mathbf{d}}} \\ \ddot{\boldsymbol{\lambda}} \\ \ddot{T} \end{Bmatrix} + \begin{bmatrix} -\mathbf{R}^{\mathbf{gl}}(\tilde{\mathbf{d}})\mathbf{A_2}(\tilde{\mathbf{d}}) & \mathbf{0} & 0 \\ -\mathbf{B_2} & \mathbf{I} & 0 \\ \mathbf{0} & \mathbf{0} & \tau_T \end{bmatrix} \begin{Bmatrix} \dot{\tilde{\mathbf{d}}} \\ \dot{\boldsymbol{\lambda}} \\ \dot{T} \end{Bmatrix}$$
$$+ \begin{bmatrix} -\mathbf{R}^{\mathbf{gl}}(\tilde{\mathbf{d}})\mathbf{A_3}(\tilde{\mathbf{d}}) & -\mathbf{R}^{\mathbf{gl}}(\tilde{\mathbf{d}})\mathbf{A_4}(\tilde{\mathbf{d}}) & 0 \\ -\mathbf{B_3} & -\mathbf{B_4} & 0 \\ \mathbf{0} & \mathbf{0} & 1 \end{bmatrix} \begin{Bmatrix} \tilde{\mathbf{d}} \\ \boldsymbol{\lambda} \\ T \end{Bmatrix} + \begin{Bmatrix} \mathbf{F_{int}}(\tilde{\mathbf{d}}, T) \\ \mathbf{0} \\ 0 \end{Bmatrix} = \begin{Bmatrix} \mathbf{0} \\ \mathbf{0} \\ H_{in} \end{Bmatrix}, \tag{13}$$

for which $H_{in}(t) = R_r i^2(t) + T_{env}$, $\mathbf{A_{(1\ldots4)}}$ and $\mathbf{B_{(1\ldots4)}}$ are the global aerodynamic matrices, $\mathbf{R^{gl}}$ is the global transformation matrix due to the follower forces assumption, and $\boldsymbol{\lambda}$ is the global lag states vector. Furthermore, $\tilde{\mathbf{d}}$ is the global structural displacement vector, $\mathbf{M}$ is the global mass matrix, and $\mathbf{F}_{\text{int}}$ is the global, nonlinear internal forces vector.

A great emphasis must be placed on the aerodynamic matrices $\mathbf{A_2}$, $\mathbf{A_3}$, $\mathbf{A_4}$, and $\mathbf{B_1}$ in Eq. 13. Notice that those matrices are nonlinearly dependent on the global displacements vector $\tilde{\mathbf{d}}$ as a

consequence of the stall model assumed. On the other hand, matrices $\mathbf{A_1}$, $\mathbf{B_2}$, $\mathbf{B_3}$, and $\mathbf{B_4}$ are independent on the stall model and thereby constant. In other words, the latter are dissociated from circulatory flow effects.

The aerothermoelastic problem formulated above gathers a remarkable collection of nonlinear phenomena of different core sources. As a major consequence, the proposed model outreaches high levels of complexity and non-linearity, as per can be observed in Eq. 13. The set of nonlinear equations derived still holds a striking relation between accuracy and computational costs. For that, a numerical solver based on the juncture of the Newmark and Newton-Raphson methods is applied. The first method is used to integrate the differential equations of motion over the time, whereas the second method is used for each time step to iterate the displacements until a solution is found.

Attention must be placed here on the fact that external dependencies of the dynamic equilibrium equation are not taken into account in the derivation process of the dynamic tangent stiffness matrix used within the Newton-Raphson method. This approach enhances the performance of the proposed methodology, and it is performed to handle the stall effects and to calculate the sectional properties of the hybrid wings.

3 RESULTS

As a first attempt to evaluate the behavior of the smart, hybrid structures proposed here, a quasi-static benchmark of a hybrid material experiencing an increasing SMA temperature is analyzed. This case was implemented to evaluate the effectiveness of SMA wires to induce stiffening effects capable of changing the static response of a hybrid beam.

The mentioned case consists of a cantilever hybrid beam subjected to a concentrated transversal load $P = 2EI(24\,^{\circ}\mathrm{C})/L^2$ at its free end. Figure 6 depicts the beam deformations for the different temperatures; moreover, the correlated bending Young's modulus $\overline{E}^b$ are shown. It was considered a hybrid beam with length $L = 3.2$ m, six-layer layup $[-45, 0, 45]_{\mathrm{S}}$, layer thickness $t_k = 0.19$ mm, constituents volume fractions $V_f = V_{sma} = 25\%$ and $V_m = 50\%$, and the constituents mechanical properties shown in Table 1.

Given a hybrid beam undertaking an end load along with the associated SMA temperature, the Newton-Raphson method was used to iterate the displacements until converged deformations were found. Next, the SMA temperature was raised, while the applied load was kept constant, and a new set of beam deformations were iterated until converged. Besides, as can be noticed here, as the operating temperature increases, the consequent SMA stiffness also increases, resulting in reduced beam deflections.

After that, analyses regarding the nonlinear aerothermoelastic behavior of hybrid were performed. However, beforehand, it is essential to specify the four envelope points that define the aeroelastic boundaries of a hybrid wing: First, V_{fl}^m and V_{div}^m are the critical flutter and divergence speeds associated with the structural condition of the wing at which the SMA wires present a state of pure martensite crystallographic phase, i.e., low-temperature phase. At second, V_{fl}^a and V_{div}^a are the analogous flutter and divergence speeds related to a structural state purely austenitic or a high-temperature state.

The aerothermoelastic cases addressed here were accomplished by assuming hybrid wings with constituents' volume fractions as $V_f = V_{sma} = 25\%$ and $V_m = 50\%$. Moreover, a layer

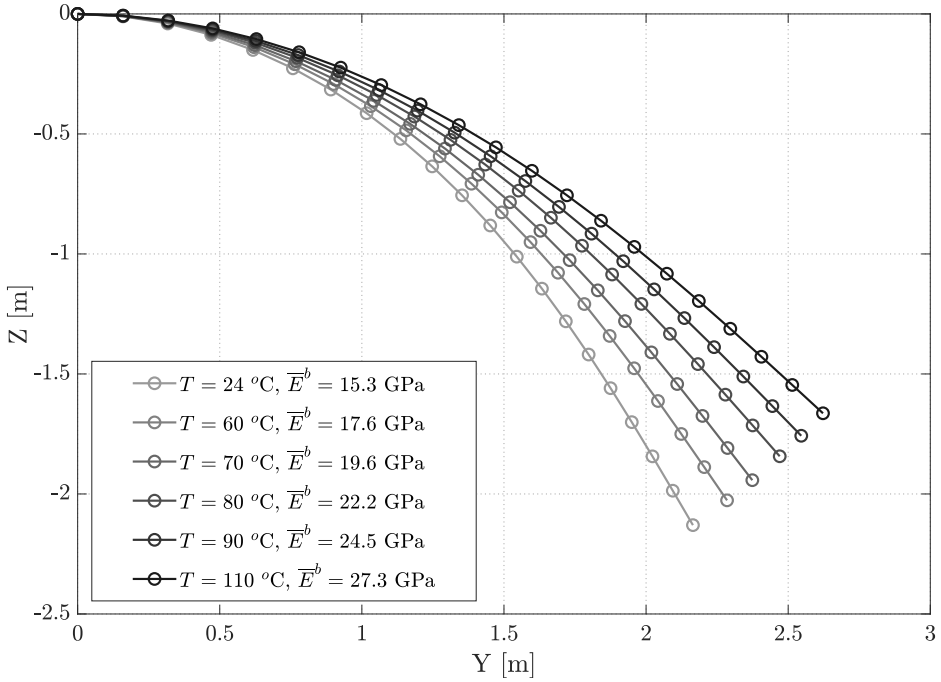

Figure 6: Hybrid beam deflections under an end load and at different SMA temperatures.

thickness of 0.19 mm, span of 350 mm, chord-length of 40 mm, and the constituents properties listed in Table 1 were considered. From the latter, the characteristic temperatures of the SMA wires made of a Ni-Ti alloy are worth-mentioning here again, such as $A_S = 45$ ^{o}C and $A_F = 90$ ^{o}C.

The first case regards the analysis of a four-layer hybrid wing with layup $[45, -45]_S$. It is assumed a store condition at the wing tip with $\Delta d_{blt} = -5$ mm in the x-direction. The associated stability boundaries found were $V_{fl}^m = 12.9$ m/s, $V_{fl}^a = 15.8$ m/s, $V_{div}^m = 26.1$ m/s, and $V_{div}^a = 36.0$ m/s. Figure 7 displays the mid-span transversal displacement w_{mid} and tip torsion angle θ_{tip} resulting from the case at $V = 15$ m/s. At the beginning, no input in the electric current was applied. The wing started thus presenting LCO as a consequence of the coupling between the second bending and first torsion modes of vibration. Later, at time $t = 70$ s, a step change of magnitude 3 A in the electric current was employed, thus inducing an additional stiffness to the system. This growth in rigidity was sufficient to suppress the oscillations.

Tailoring this type of smart structure involves a series of parameters. Therefore, aiming at improving our knowledge on this topic, Fig. 8 shows the influence of temperature and lamina orientation on the aeroelastic stability of a hybrid wing. This plot contains a 3D representation of the critical flutter speed of a hybrid wing with layup $[\phi, -\phi]_S$ and ballast condition $\Delta d_{blt} = -5$ mm, while the temperature T and ply angle ϕ are varied.

The 3D plot reveals maximum local points for ply angles ϕ about ± 45. This result can be explained by the fact that the wing also presents maximum torsional stiffness for $\phi = \pm 45$, which results in a maximized relation between the first torsion mode and the first of second bending modes. Remarks must be also placed on the central region of the 3D curve, whereat a noticeable set of points appears, in red. These points represent conditions for which the divergence speed is lower than the associated flutter speed, as a result of lower torsional stiffness conditions.

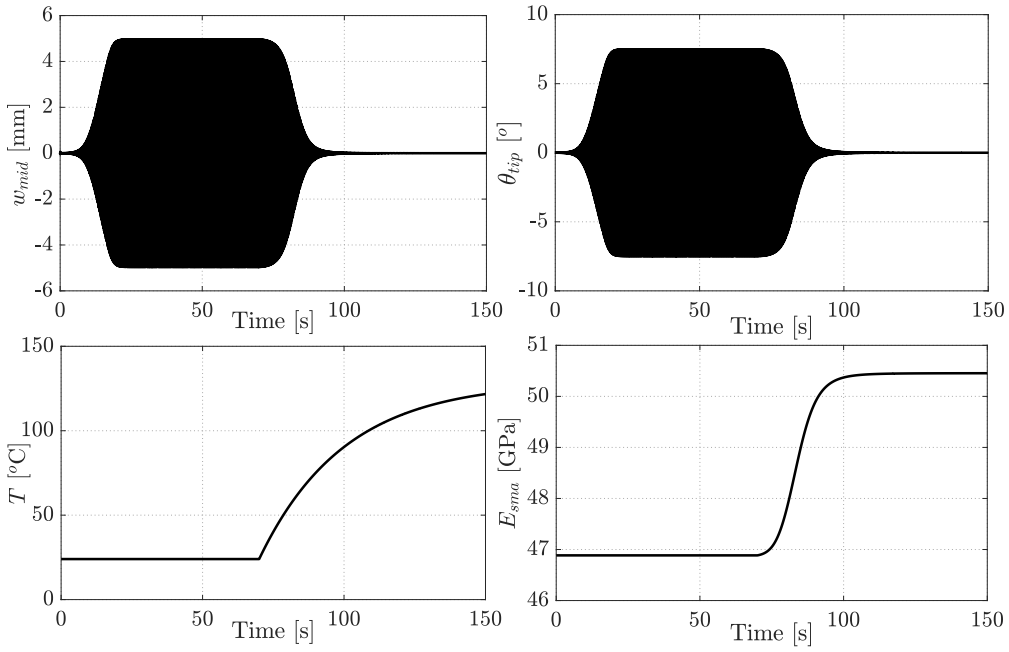

Figure 7: Aerothermoelastic response of a hybrid wing with layup $[\pm 45]_S$ and $V = 15$ m/s.

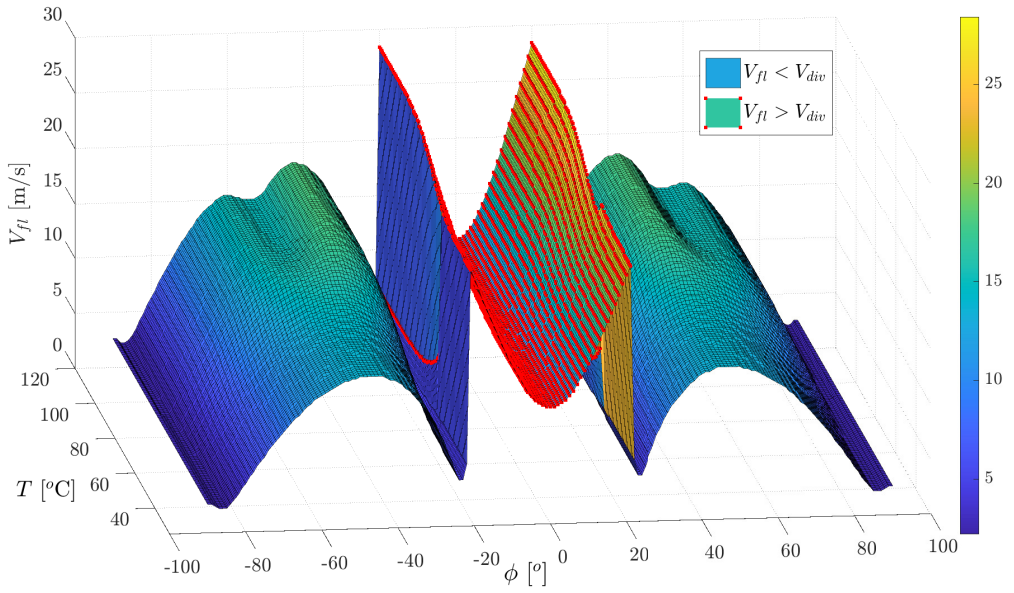

Figure 8: Effects of temperature and ply angle on the critical flutter speed of a hybrid wing.

Intending to investigate one of the red points shown in the previous plot, a simulation was performed by assuming $\phi = 0^o$. The following envelope boundaries were then found: $V_{fl}^m = 10.6$ m/s, $V_{fl}^a = 12.3$ m/s, $V_{div}^m = 10$ m/s, and $V_{div}^a = 10.1$ m/s. The analysis was simulated assuming an airspeed of 11.5 m/s, i.e., $V_{div}^m < V_{div}^a < V < V_{fl}^m < V_{fl}^a$.. The outcomes from this case are depicted in Fig. 9. Here, the wing is initially ruled by divergence effects, and it responds with sustained vibrations afterwards, caused by components of a flutter instability in the response. These oscillations are resulting from the coupling between the first torsion and the first bending modes. After the SMAs being heated, the resulting stiffening effects could suppress the oscillations.

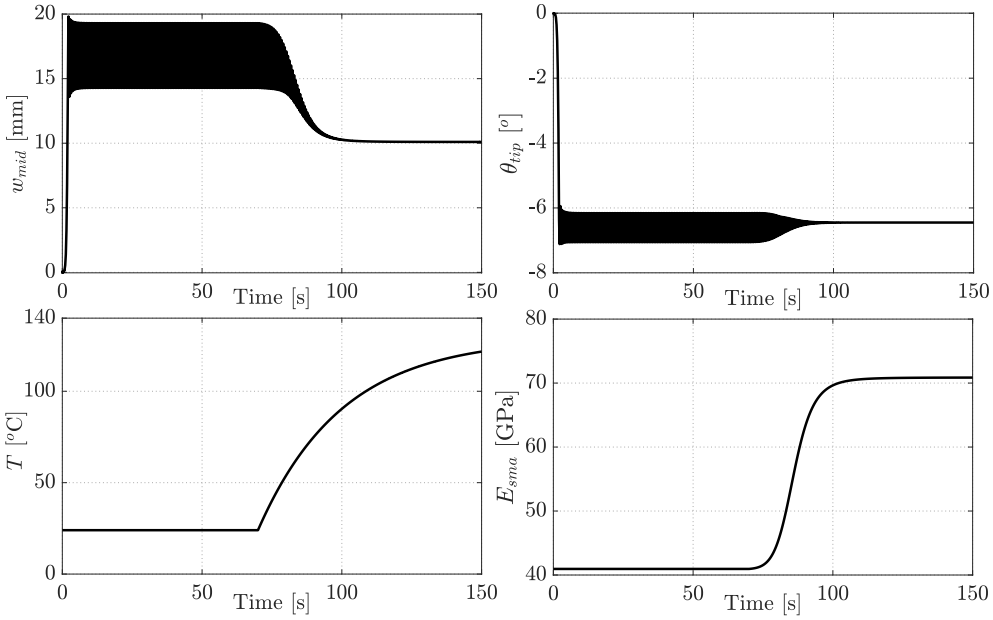

Figure 9: Aerothermoelastic response of a hybrid wing performed at 11.5 m/s.

4 CONCLUSIONS

The present work developed the so-called nonlinear aerothermoelastic model of flexible hybrid wings connected with the thermal dynamics of SMAs. This problem involves nonlinearities of diverse sources, including geometrical, aerodynamic, and material. Geometrical nonlinearities were taken into account via a Timoshenko beam element under large deflections and rotations. Material nonlinearities were enclosed by employing a thermal-elastic model of SMA materials within a micromechanical method for multi-phasic composites. Meanwhile, aerodynamic nonlinearities were accounted via an unsteady strip theory method in the time-domain, together with both stall and follower aerodynamic forces models.

The numerical simulation regarding hybrid SMA-composite beams applied for a static benchmark was performed by assuming different SMA temperatures. The outcome showed a great capability of hybrid structures for shape control. This can be performed by encountering a suitable relation between loads and the temperature of the SMAs. Aerothermoelastic cases of flexible hybrid wings with diverse layups were also tested at different envelope points. In these cases, the stiffening effects induced by the SMA heating process via Joule's effect reduced both flutter oscillations and divergence amplitudes. These results instantiate the implementation of aeroelastic control approaches that use hybrid materials.

To conclude, aeroelastic optimization is an integral part of formal procedures for aircraft designers. The possibility of using long hybrid wings to improve aircraft performance enables the use of variable structural features, which may provide the most suitable response for the different flight conditions. The additional parameter combinations offered by these smart materials must then be taken into account in order to design hybrid wings. On the other hand, further parameters and effects might be also investigated in future works, such as SMA hysteresis, and different angles of attack and sweep angle.

5 REFERENCES

[1] Jung, Y. C. and Cho, J. W. (2010). Application of shape memory polyurethane in orthodontic. *Journal of Materials Science: Materials in Medicine*, 21(10), 2881–2886.

[2] Loughlan, J., Thompson, S., and Smith, H. (2002). Buckling control using embedded shape memory actuators and the utilisation of smart technology in future aerospace platforms. *Composite structures*, 58(3), 319–347.

[3] Kim, N.-G., Han, M.-W., Iakovleva, A., et al. (2020). Hybrid composite actuator with shape retention capability for morphing flap of unmanned aerial vehicle (uav). *Composite Structures*, 243, 112227.

[4] C. Bil, E. A., K. Massey (2013). Wing morphing control with shape memory alloy actuators. *Journal of Intelligent Material Systems and Structures*, 24(7), 879–898.

[5] Leal, P. and Savi, M. (2018). Shape memory alloy-based mechanism for aeronautical application: Theory, optimization and experiment. *Aerospace Science and Technology*, 76, 155–163.

[6] O.D. de Matos Jr., S. C., M.V. Donadon (2017). Aeroelastic behavior of stiffened composite laminated panel with embedded sma wire using the hierarchical rayleigh–ritz method. *Composite Structures*, 181, 26–45.

[7] Sofla, A., Meguid, S., Tan, K., et al. (2010). Shape morphing of aircraft wing: Status and challenges. *Materials & Design*, 31(3), 1284–1292.

[8] Silva, G. C., Silvestre, F. J., Donadon, M. V., et al. (2017). Active and passive control for acceleration reduction of an aeroelastic typical wing section. *Journal of Vibration and Control*, 24(13), 2673–2687.

[9] J.M. Jani, A. S. M. G., M. Leary (2014). A review of shape memory alloy research, applications and opportunities. *Materials & Design (1980-2015)*, 56, 1078–1113.

[10] Silva, G. C., Silvestre, F. J., and Donadon, M. V. (2022). A nonlinear aerothermoelastic model for slender composite beam-like wings with embedded shape memory alloys. *Composite Structures*, 287, 115367.

[11] S.A. Aquino, M. S. I. A. S., J.M. Borges (2010). Controle de vibração de um sistema sob desbalanceamento rotativo utilizando atuador de liga com memória de forma. *Proceedings of the VI National Congress of Mechanical Engineering*.

[12] Donadon, M. and de Faria, A. (2016). Aeroelastic behavior of composite laminated shells with embedded sma wires under supersonic flow. *Aerospace Science and Technology*, 52, 157–166.

[13] Halpin, J. C. (1969). Effects of environmental factors on composite materials. Tech. rep., Air Force Materials Lab Wright-Patterson AFB OH.

[14] Wagner, H. (1925). Über die entstehung des dynamischen auftriebes von tragflügeln. *ZAMM-Journal of Applied Mathematics and Mechanics/Zeitschrift für Angewandte Mathematik und Mechanik*, 5(1), 17–35.

[15] Jones, R. T. (1938). Operational treatment of the nonuniform-lift theory in airplane dynamics.

[16] Jr, E. Y. (1966). Modified-strip-analysis method for predicting wing flutter at subsonic to hypersonic speeds. *Journal of Aircraft*, 3(1), 25–29.

[17] Silvestre, F. J. and Luckner, R. (2015). Experimental validation of a flight simulation model for slightly flexible aircraft. *AIAA Journal*, 53(12), 3620–3636.

[18] Pelletier, A. and Mueller, T. (2000). Low reynolds number aerodynamics of low-aspect-ratio, thin/flat/cambered-plate wings. *Journal of Aircraft*, 37(5), 825–832.

COPYRIGHT STATEMENT